Models of a 750 GeV quarkonium and the LHC excesses

Koichi Hamaguchi[1,2] and Seng Pei Liew[1]

[1]*Department of Physics, University of Tokyo, Tokyo 113-0033, Japan*
[2]*Kavli Institute for the Physics and Mathematics of the Universe (Kavli IPMU),*
University of Tokyo, Kashiwa 277-8583, Japan

We investigate models involving a vectorlike quark (X), which forms a 750 GeV bound state and reproduces the observed diphoton signals at the LHC, in connection with other excesses in the LHC data. An exotic hypercharge of $-4/3$ is required to fit the signal cross section, which indicates that there is an additional particle(s) that mediates the decay of X in the full theory. We find that introducing an SU(2) doublet vectorlike quark of mass around 600 GeV in our UV-complete framework can accommodate not only the diphoton but also the on-Z excess (and potentially a slight excess in the monojet events). Our models also include a dark matter candidate. The most useful way to probe the models at the LHC is via monojet searches. The relic dark matter density is largely determined by coannihilation effects, and indirect detection of dark matter annihilation signals is the alternative and complementary probe of our models.

I. INTRODUCTION

The ATLAS and CMS collaborations have recently analyzed the Large Hadron Collider (LHC) data at a center-of-mass energy of 13 TeV (run 2) and reported an excess of diphoton events at about 750 GeV [1,2]. The ATLAS shows a local (global) significance of 3.9σ (2.0σ), while the CMS reported a local (global) significance of 2.8–2.9σ ($<1\sigma$) depending on the spin hypothesis recently [3,4].

Among many possible interpretations, one of the most attractive scenarios is the 750 GeV quarkonium, i.e., a QCD bound state of heavy vectorlike quark with a mass of about 375 GeV [5–9]. Unlike many other diphoton models, the necessary ingredients for the diphoton excess in this scenario is extremely simple; just the existence of the vectorlike quark X with a small width, $\Gamma_X \ll \Gamma(S \to \gamma\gamma) \simeq \mathcal{O}(\mathrm{MeV})$, can lead to a diphoton resonance, and it does not require an additional 750 GeV singlet field nor new strong dynamics other than the Standard Model (SM) gauge group. In particular, it was shown in Refs. [8,9] that the diphoton signal rate can be explained by a bound state of vectorlike quarks X which transforms as $(\mathbf{3}, \mathbf{1}, -4/3)$ under the $SU(3) \times SU(2) \times U(1)_Y$ of the SM gauge groups.

Although the setup above for the diphoton signal is very simple, it cannot be the full theory. In particular, the theory must allow the decay of X to avoid the severe collider bound on the long-lived colored particle [10]. In Refs. [8,9], the decay of X into multijets (and missing energy) was discussed. In particular, Ref. [8] studied the case that X decays via higher dimensional operators, assuming that the decay products contain a dark matter (DM) final state with a mass close to that of the X. It was shown that the current collider and cosmological bounds on X can be evaded if the mass difference between X and the DM is about $30 \sim 50$ GeV.

In this paper, we propose explicit renormalizable models to complete this scenario. As the vectorlike quark X in this scenario has an exotic quantum number, it cannot have a renormalizable interaction with the SM quarks. Therefore, an additional colored particle must be introduced to mediate the decay of X. We investigate the possibility that such a colored mediator, which we denote by Y, is an SU(2) doublet vectorlike quark with a SM quantum number $(\mathbf{3}, \mathbf{2}, -5/6)$. The doublet consists of two quarks with charges $-4/3$ and $-1/3$, and it can couple to both the X and the down-type SM quarks, mediating the decay of the X field.

Interestingly, we have found that the decay of the lower component of the Y into X may also explain the ATLAS on-Z excesses [11,12].[1] The on-Z analyses are supersymmetry (SUSY) searches conducted to look for events with dilepton, jets and missing energy. At 8 (13) TeV, 29 (21) events are observed while the expected SM background events are 10.6 (10.3), corresponding to a deviation of 3.0σ (2.2σ) from SM. We show that the on-Z excess can be explained assuming that the vectorlike quarks have masses $m_X \simeq 375$ GeV and $m_Y \simeq 600$–700 GeV and the decay of X contains a large missing energy.

In the second part of this paper, we propose two explicit models. Since the on-Z excess requires missing energy, which also relaxes the constraints from the X search, we introduce a dark matter field in addition to the vectorlike quarks X and Y. In the first model, we consider an inert

---

[1]It is noted that the CMS Collaboration has reported results consistent with SM predictions in the same channel. It could be due to the incompatibility between the collaborations at estimating the number of background events, as emphasized in Ref. [13]. In this work, the ATLAS excesses are interpreted as a contribution originated from BSM physics. See Refs. [13–26] for previous theoretical efforts interpreting the excess.

doublet dark matter, while in the second model, a singlet scalar dark matter is introduced together with yet another vectorlike quark. We investigate LHC constraints as well as the dark matter phenomenology of these models. It is worth noting that monojet searches are of particular significance in our mass-degenerate scenarios, coinciding with the observation that there is a slight (1σ) excess in the 13 TeV monojet signal region [27]. Therefore, LHC anomalies (on-Z, monojet) other than the diphoton resonance may be incorporated within our UV-complete framework.

The rest of the paper is organized as follows. In Sec. II, we briefly review the scenario of the 750 GeV quarkonium, in particular the case with a vectorlike quark X with a hypercharge $Y_X = -4/3$. In Sec. III, we introduce a new SU(2) doublet vectorlike quark Y to complete the model and investigate its implication on the ATLAS on-Z excesses. In Sec. IV, we propose explicit models and study LHC constraints and dark matter phenomenology in each model. A summary and discussion are given in Sec. V. The details of the LHC analyses are described in Appendix A, and some analytic formulas for models in Sec. IV are presented in Appendix B.

II. 750 GeV QUARKONIUM AND THE DIPHOTON EXCESS

In this section, we briefly review the scenario of the 750 GeV quarkonium, which is a bound state of vectorlike quarks X with a mass of $m_X \simeq 375$ GeV. When a pair of the X quarks is produced near the threshold energy, it can form a color-singlet, S-wave bound state, and the production cross section is enhanced. In Ref. [8], the diphoton cross section is calculated for various hypercharges Y_X, assuming that X is a color triplet and SU(2) singlet, and it was shown that the case of $|Y_X| = 4/3$ explains the best the diphoton excess. In Ref. [9], the cross section is calculated for various constituent particles—for spins 0, 1/2, and 1, various color representations, and different electromagnetic charges. A color-triplet fermion with electric charge $-4/3$ is among the best candidates, together with other possibilities such as the color-triplet scalar with charge $-4/3$ or $5/3$ and color-sextet scalar with charge $-2/3$.

In this paper, we consider the case when the X has a quantum number $(\mathbf{3}, \mathbf{1}, -4/3)$ under the SU(3) × SU(2) × U(1)$_Y$ of the SM gauge group. In Refs. [8,9], the $\gamma\gamma$ production cross section through the bound state is estimated as

$$\sigma(pp \to S_0(X\overline{X}) \to \gamma\gamma) \simeq \begin{cases} 5.7 \text{ fb } [8], \\ 4.7 \text{ fb } [9], \end{cases} \quad (1)$$

up to (large) uncertainties discussed there.[2]

---

[2]In Ref. [9], the QCD binding potential is approximated to be Coulomb-like [28]. Reference [8] makes use of a different QCD potential and includes the effects of the electric force.

The decay width of the 750 GeV bound state in this scenario is around 6 MeV [8], indicating a narrow-width scalar resonance. This setup predicts other bound state signals (dijet, diboson, etc.) as well, but they are thus far not strongly constrained. It should be noted that the decay rate of the constituent fermion X should be smaller than that of the bound state in order to enhance the diphoton signal. This amounts to the condition $\Gamma_X \lesssim \mathcal{O}(1)$ MeV, which, as will be discussed in the following sections, can be easily satisfied in our models.

III. VECTORLIKE QUARKS AND ATLAS ON-Z EXCESS

As mentioned in the Introduction, the setup of the previous section cannot be the complete model and X should have an additional interaction which allows its decay. In Refs. [8,9], the decay of X into multijets (and missing energy) was discussed without specifying the UV completion of the model. In this paper, we propose explicit renormalizable models to complete the scenario. As in Ref. [8], we assume that the decay of X contains a DM in the final state.

Because of the exotic charge $Y_X = -4/3$, the X quark cannot have a renormalizable interaction with the SM field. Therefore, a new colored field should be introduced to mediate its decay. We consider a vectorlike fermion for such a new colored mediator and denote it by Y. Assuming that X and Y are coupled via a Yukawa coupling with the SM Higgs, Y should be an SU(2) doublet with a hypercharge $-5/6$ or $-11/6$. We consider the former case since it can couple to the SM down-type quarks, while the latter case needs further additional colored fields, i.e.,

$$Y = \begin{pmatrix} B' \\ X' \end{pmatrix}_{-5/6}, \quad (2)$$

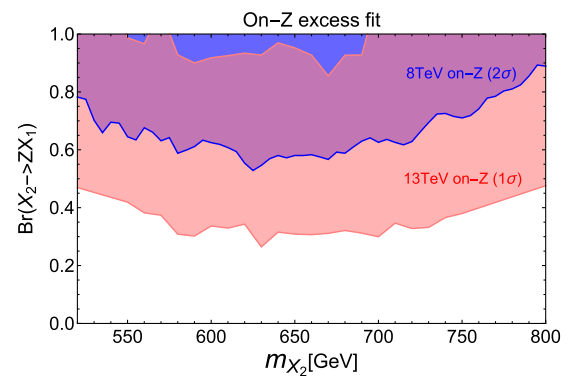where B' and X' have electric charges $-1/3$ and $-4/3$, respectively. The interaction is then given by

FIG. 1. The on-Z excess fit on the Br$(X_2 \to X_1 Z)$ and X_2 mass plane for $m_{X_1} = 375$ GeV. The blue region shows the fit of run 1 data at statistical significance of 2σ, while the pink band indicates the fit of run 2 data at 1σ.
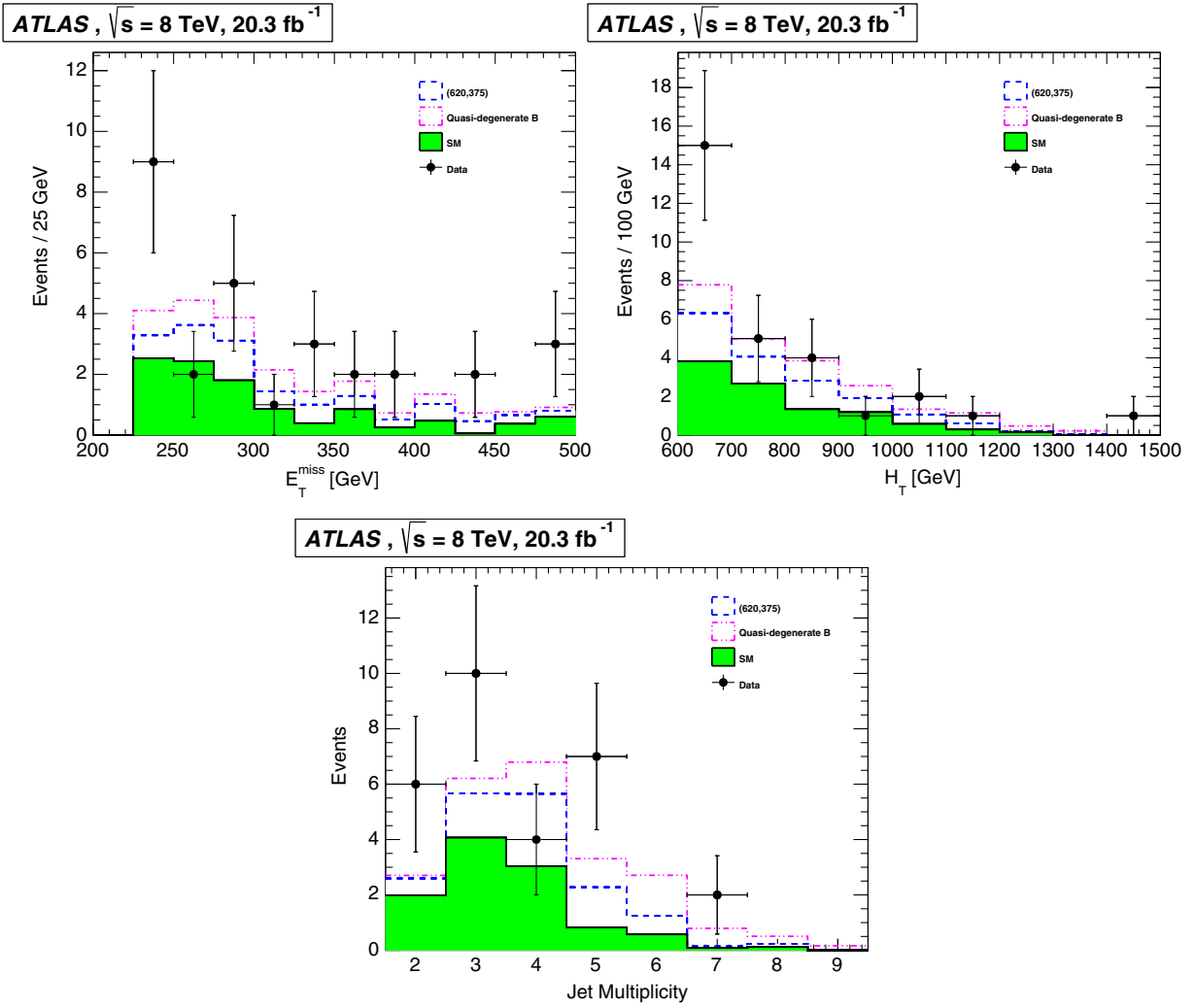
FIG. 2.   (from top left to bottom) Event distribution of E_T^{miss}, H_T and jet multiplicity in the on-Z signal region of run 1 (8 TeV) [11], which contains a pair of electron or muon in the final state. Observed events (black dots) are compared with the expected event distribution for the model point with $m_{X_2} = 620$ GeV, $m_{X_1} = 375$ GeV, and $\mathrm{Br}(X_2 \to X_1 + Z) = 0.8$ (blue) and the "quasidegenerate B" scenario (pink), on top of the expected SM background (green).

$$-\mathcal{L}_{\mathrm{int}} = (\overline{Y}H)(\lambda_X + \lambda_{X5}\gamma_5)X + \mathrm{H.c.}, \qquad (3)$$

where $H = (H^+, H^0)^T$ is the SM Higgs doublet and $(\overline{Y}H) = \overline{B'}H^+ + \overline{X'}H^0$. Here and throughout the paper, we assume $\lambda_{X5} = 0$ for simplicity. As we shall see in the explicit models discussed in the next section, the Y field can couple to the SM quarks and the DM field directly or indirectly, allowing the decay of the X field through the Y.

Before discussing the details of the models in the next section, let us discuss the possible explanation of the ATLAS on-Z excess in this scenario. The interaction in (3) causes a mixing between X and X', resulting in mass eigenstates X_1 and X_2. The heavier one can decay into the lighter one, emitting a Z boson or the Higgs boson:

$$X_2 \to X_1 + Z/h. \qquad (4)$$

As we will see, this decay channel leads to a signal with $Z + \mathrm{jets} + \mathrm{missing}$ energy, which may explain the ATLAS on-Z excess.

The major features of the ATLAS on-Z analysis are as follows. The final state must include at least a pair of opposite sign same flavor (OSSF) leptons (electron or muon) with invariant mass close to the Z boson mass. The required missing transverse energy is $E_T^{\mathrm{miss}} > 225$ GeV. At least two signal jets (reconstructed using the anti-k_t algorithm [29]) are required, and a cut of $H_T > 600$ GeV, where H_T is the scalar sum of jet p_T, is applied to the final state (see Appendix A for further details). Assuming that the number of observed events in the signal region follows the Poisson distribution, and by adding the statistical uncertainty as well as the systematic uncertainty in quadrature, the number of excessive events due to new physics are
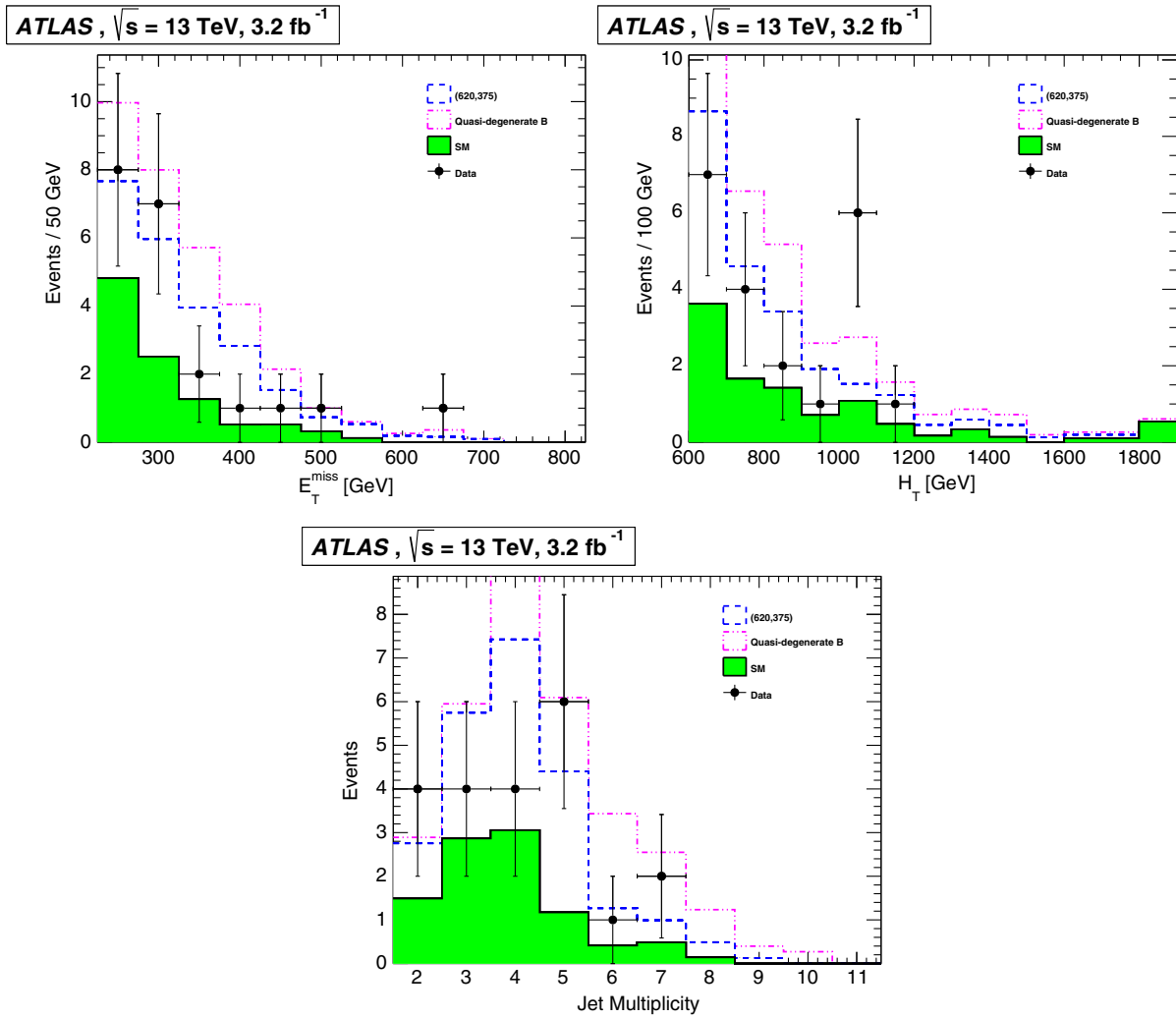
FIG. 3.   (from top left to bottom) Event distribution of E_T^{miss}, H_T and jet multiplicity in the on-Z signal region of run 2 (13 TeV) [12], which contains a pair of electron or muon in the final state. Observed events (black dots) are compared with the expected event distribution for the model point with $m_{X_2} = 620$ GeV, $m_{X_1} = 375$ GeV, and $\mathrm{Br}(X_2 \to X_1 + Z) = 0.8$ (blue) and the "quasidegenerate B" scenario (pink), on top of the expected SM background (green).

$$N_{\mathrm{BSM}} = 18.4 \pm 6.3 \quad \text{in the run 1 analysis,} \qquad (5)$$

$$N_{\mathrm{BSM}} = 10.7 \pm 5.1 \quad \text{in the run 2 analysis.} \qquad (6)$$

We have used the following pipeline to estimate the on-Z excess fit of our model: MadGraph 5 v2.2.3 [30,31] for event generation, Pythia 6.4 [32] for parton shower and Checkmate [33,34] for analysis implementations. Checkmate utilizes Delphes 3 [35] (which has FastJet incorporated [36,37]) for detector simulations.

We have generated three samples $(pp \to X_2 \overline{X}_2 \to X_1 \overline{X}_1 + ZZ/Zh/hh)$ and made appropriate rescaling to vary the branching ratio of $X_2 \to X_1 Z$ while fitting the on-Z excess. In addition, the process $pp \to B' \overline{B'} \to X_1 \overline{X}_1 + W^+ W^-$ is also generated and included in our analysis. Our model is implemented using Feynrules v2.3.1 [38], and the

vectorlike quark pair production cross section is estimated up to next-to-next-to leading order accuracy using Hathor v2.0 [39].

The result of our fit is shown in Fig. 1. Here, X_1 is assumed to decay into DM (E_T^{miss}) accompanied by two jets, while the mass splitting between X_1 and DM is set to be 40 GeV. Jets from the decay of X_1 are relatively soft, and the on-Z result is insensitive to the details of X_1 decay. It can be seen that $\mathrm{Br}(X_2 \to X_1 Z) \gtrsim 0.6$ is necessary in order to fit the run 1 on-Z excess at 2σ. The requirement to fit the run 2 excess is looser, with $\mathrm{Br}(X_2 \to X_1 Z) \gtrsim 0.4$ at 1σ. The reason is twofold: (i) the production cross section is enhanced at 13 TeV, and (ii) the observed number of excessive events is smaller in run 2.

In Figs. 2 and 3, we show the predicted E_T^{miss}, H_T and jet multiplicity distribution for a benchmark point on top of expected SM background as compared to the run 1 and run

2 data, respectively. As the parameters of the benchmark point, we have chosen $m_{X_2} = 620$ GeV, $m_{X_1} = 375$ GeV and $\mathrm{Br}(X_2 \to X_1 + Z) = 0.8$.[3] The blue dashed line shows the contributions from $X_2 \to X_1 + Z/h$ (and $B' \to X_1 + W$), which produces $N_{\mathrm{BSM}} = 8.5(13.4)$ events at 8 (13) TeV. As shown in Fig. 1, the contribution at 8 TeV is fitted up to 2σ compared with the excess, while the fit is reasonably better at 13 TeV (within 1σ).

As an illustration, we also show the distributions for another benchmark point, "quasidegenerate B," by pink dashed lines. Here, we have an additional particle B or B_2 in the mass eigenstate, with $m_{B_2} = 705$ GeV (see Sec. IV C for details of model building). B_2 decays solely to WX_2, as other decay channels are kinematically closed. This "quasidegenerate B" scenario produces $N_{\mathrm{BSM}} = 10.7(17.2)$ events at 8 (13) TeV, which gives more signal events than the benchmark point discussed above for both run 1 and run 2 data.

We have also checked other relevant collider analyses which potentially constrain our model. It is found that the multijet plus $E_{\mathrm{T}}^{\mathrm{miss}}$ search [40] gives the most stringent constraint, though our benchmark scenarios are still allowed. Furthermore, the direct pair production of X_1 can be constrained by monojet searches. This constraint will be further discussed in the next section.

IV. MODELS FOR 750 GeV DIPHOTON AND ON-Z EXCESSES

In this section, we introduce two explicit models which can explain the 750 GeV diphoton and on-Z excesses simultaneously. The matter contents of the models are summarized in Table I.
  (1) In the first model, we introduce an inert doublet η in addition to X and Y. We assume $m_Y > m_X > m_\eta$.
  (2) In the second model, a singlet scalar dark matter ϕ is introduced together with yet another vectorlike quark B. We consider two cases:
      (a) $m_Y > m_X > m_B > m_\phi$ (light B),
      (b) $m_B > m_Y > m_X > m_\phi$ (heavy B).

Generically, our models contain a colored mediator which couples to DM as well as SM quarks. Such quark generation-dependent couplings cannot be arbitrary due to stringent constraints on the first and second quark generation couplings from flavor changing neutral current (FCNC) processes.[4] We choose the couplings to the third generation to be the dominant ones in order to avoid these constraints.

A. Model $XY\eta$

From the matter content in Table I, the most generic renormalizable Lagrangian is

TABLE I. Matter contents of the two models. X, Y, and B are Dirac fermions, η is a complex scalar, and ϕ is a real scalar. All fields are odd under Z_2 parity.

		Model	
Model $XY\eta$	$(SU_3, SU_2)_{U_{1Y}}$	$XYB\phi$	$(SU_3, SU_2)_{U_{1Y}}$
X	$(\mathbf{3}, \mathbf{1})_{-4/3}$	X	$(\mathbf{3}, \mathbf{1})_{-4/3}$
$Y = (B', X')^T$	$(\mathbf{3}, \mathbf{2})_{-5/6}$	$Y = (B', X')^T$	$(\mathbf{3}, \mathbf{2})_{-5/6}$
$\eta = (\eta^+, \eta^0)^T$	$(\mathbf{1}, \mathbf{2})_{1/2}$	B	$(\mathbf{3}, \mathbf{1})_{-1/3}$
		ϕ	$(\mathbf{1}, \mathbf{1})_0$

$$\mathcal{L} = \mathcal{L}_{\mathrm{SM}} + \sum_{F=Y,X} \overline{F}(i\slashed{D} - m_F)F + |D_\mu \eta|^2 - m_\eta^2 |\eta|^2$$
$$- V(H, \eta) - (\overline{Y}H)(\lambda_X + \lambda_{X5}\gamma_5)X$$
$$- y_{\eta i}\overline{d_{Ri}}P_L(Y \cdot \eta) + \mathrm{H.c.} \quad (7)$$

where $(\overline{Y}H) = \overline{B'}H^+ + \overline{X'}H^0$, $(Y \cdot \eta) = B'\eta^0 - X'\eta^+$, and d_{Ri} denotes the SM right-handed down-type quarks. For simplicity, we assume $\lambda_{X5} = 0$.[5] We further assume that Y mainly couples to the third generation quark, and take $y_{\eta 1} = y_{\eta 2} = 0$ and $y_{\eta 3} = y_\eta$. The Yukawa couplings λ_X and y_η can be taken to be real and positive by field redefinitions. As mentioned in the previous section, the X and X' are mixed through the Yukawa interaction in (7), leading to mass eigenstates X_1 and X_2. The main decay modes of the new particles are given by, assuming $m_{X_2} \simeq m_{B'} > m_{X_1} > m_\eta$ and $\lambda_X \gg y_\eta$,

$$X_2 \to \begin{cases} X_1 Z \\ X_1 h \end{cases}, \quad B' \to X_1 W, \quad X_1 \to b\eta^-,$$
$$\eta^- \to \eta^0 + \pi^-. \quad (8)$$

The mixings and decay rates of the mass eigenstate quarks are summarized in Appendix B 1.

For simplicity, we consider the case where there is no renormalizable interaction between η and the SM Higgs. The loop corrections make the neutral component slightly lighter than the charged component, i.e., $\Delta m \simeq 350$ MeV [42]. Then, the decay of η^- produces only very soft pion with a decay rate [43]

$$\Gamma(\eta^- \to \eta^0 + \pi^-) \simeq 3 \times 10^{-14} \ \mathrm{GeV} \left(\frac{\Delta m}{350 \ \mathrm{MeV}}\right)^3 \beta, \quad (9)$$

where $\beta = \sqrt{1 - (m_{\pi^-}/\Delta m)^2}$. Therefore, the η^- can be regarded as a missing particle at collider searches.

---

[3]This point corresponds to $(m_X, m_Y) \simeq (440, 560)$ GeV and $\lambda_X \simeq 0.6$. See Sec. IV and Fig. 4 for details.
[4]An example of the FCNC calculations with similar setup can be found in Ref. [41].

[5]The interaction $|H|^2|\eta|^2$ would not change our conclusion, except that the direct and indirect constraints on the DM become severer. The interaction $|H^\dagger \eta|^2$ would cause a mass splitting between charged Higgs and DM, but its contribution is smaller than the loop correction for coupling smaller than $O(0.01)$ [42].
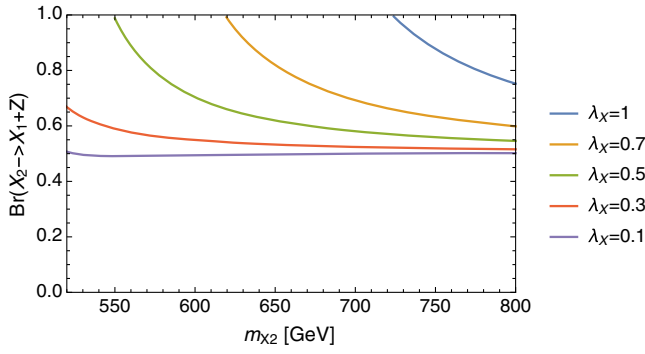
FIG. 4. The branching fraction $\mathrm{Br}(X_2 \to X_1 Z)$ as a function of m_{X_2}, for $m_{X_1} = 375$ GeV, $\lambda_X = 0.1$–1, and $y_\eta \ll \lambda_X$.

1. Diphoton and ATLAS on-Z excesses

As discussed in Secs. II and III, this model may explain the diphoton and ATLAS on-Z excesses simultaneously.
(i) The decay rate of the X_1 is given by (cf., Appendix B 1)

$$\Gamma(X_1 \to b\eta^-) \simeq 1.1 \times 10^{-7} \text{ GeV} \left(\frac{\lambda_X}{0.1}\right)^2 \left(\frac{y_\eta}{0.01}\right)^2$$

(10)

where we have taken $(m_{X_2}, m_{X_1}, m_\eta) \simeq (620, 375, 325)$ GeV as a benchmark point. Therefore, it can easily satisfy the condition for the diphoton excess, $\Gamma(X_1 \to b\eta^-) \ll \Gamma(S_0(X\bar{X}) \to \gamma\gamma) \simeq 1$ MeV, for $y_\eta \ll \lambda_X \lesssim 1$.
(ii) For the on-Z excess, in Fig. 4 we show the branching fraction $\mathrm{Br}(X_2 \to X_1 Z)$ as a function of m_{X_2}, for $m_{X_1} = 375$ GeV, $\lambda_X = 0.1$–1, and $y_\eta \ll \lambda_X$. Compared with Fig. 1, one can see that both the run 1 and run 2 excesses can be explained in a large region of parameter space.[6]

2. Other LHC constraints

Since the 375 GeV vectorlike quark X_1 decays to $\eta^- b$ with η^- decaying into a very soft pion, this decay mode could lead to final state with b-jets plus large E_T^{miss}. We make use of the acceptance times efficiency table provided by the ATLAS sbottom search [44] to estimate its constraints on this channel. The result is shown in Fig. 5. As can be seen in Fig. 5, models with large $X_1 - \eta$ mass splitting ($\gtrsim 60$ GeV) are disfavored.

The situation where X_1 decays to a soft jet and an almost mass degenerate η could avoid this collider bound, but may be constrained by monojet searches [27,45,46], which are relevant when X_1 is produced in pair and recoiled against an energetic initial state radiation (ISR). In order to study

---

[6]The region close to $\mathrm{Br}(X_2 \to X_1 Z) = 1$ corresponds to the maximal mixing, $\sin 2\theta_X \simeq 1$, where $m_X \simeq m_Y \simeq (m_{X_1} + m_{X_2})/2$. (See Appendix B 1.)
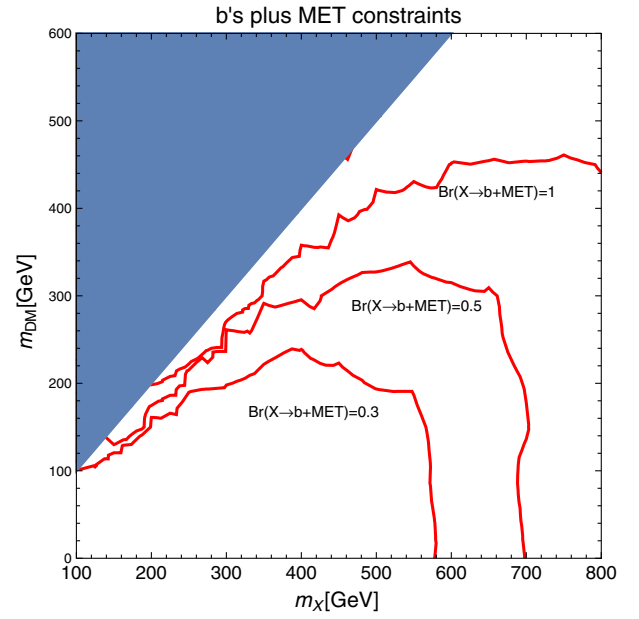

FIG. 5. b-jets plus E_T^{miss} constraints recast from auxiliary Fig. 4 of the ATLAS sbottom search [44] for different choices of decay branching ratio. The signal cross section has been normalized to that of the vectorlike fermion pair production cross section calculated using HATHOR.

the monojet constraints, again we generate samples of monojet events with MADGRAPH plus PYTHIA. Jet-parton matching is performed using the MLM scheme [47–49]. We use the parameter $r_{\mathrm{obs}} \equiv (N_{\mathrm{sig}} - 1.96\Delta N_{\mathrm{sig}})/N_{\mathrm{obs}}^{95\%}$ to estimate the 95% exclusion limits on our model (the model is considered excluded if $r_{\mathrm{obs}} > 1$), with N_{sig} being the number of BSM events in the signal region, ΔN_{sig} the uncertainty, $N_{\mathrm{obs}}^{95\%}$ the observed 95% limit on the event number given by the experimental collaborations.

Our results are presented on the $X_1 - \eta$ mass splitting versus X_1 mass plane as in Fig. 6. We find that the ATLAS 13 TeV monojet search (signal region SR2jm) gives the most stringent constraint [27], followed by signal regions SR6 and SR5 of the 8 TeV monojet analysis [46]. Our model (with $m_{X_1} \simeq 375$ GeV) is still viable for mass splitting larger than 40 GeV. Finally, we note that currently there is a slight excess of around 1σ in SR2jm. It is exciting to point out that our model could as well accommodate the excess, though the excess is appreciably less significant than that of diphoton and on-Z. This channel should definitely be studied rigorously in the future runs.

3. Dark Matter

The properties of η are completely determined by SM gauge symmetry as we consider the case where there is no renormalizable interaction between η and the SM Higgs. Since there is no direct couplings to quarks or gluons, it is difficult to probe this model with direct detection experiments.
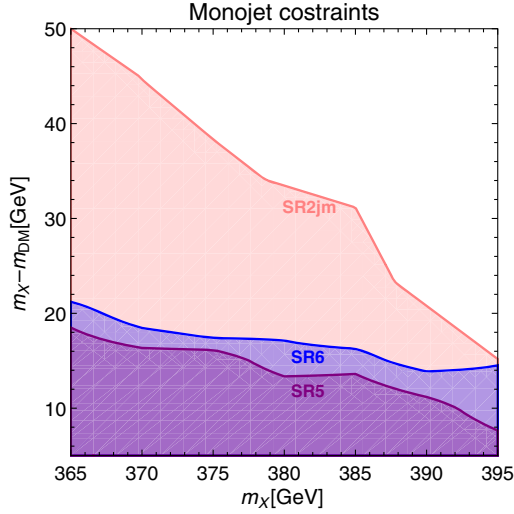
FIG. 6. Monojet constraints on the $XY\eta$ model. The most sensitive signal regions are SR2jm (pink) [27], SR6 (blue) and SR5 (purple) [46]. Below the thick line of each signal region, the parameter region is excluded.

On the other hand, DM annihilates dominantly to electroweak gauge bosons, and the s-wave annihilation cross section is given as [42]:

$$\sigma v \simeq 9 \times 10^{-26} \text{ cm}^3 \text{ s}^{-1} \left(\frac{m_{DM}}{335 \text{ GeV}} \right)^{-2}, \qquad (11)$$

while the search on dwarf spheroidal galaxies (dSphs) for gamma rays with six years of Fermi-LAT data places a 95% confidence level limit of $\sigma v \lesssim 8.5 \times 10^{-25}$ cm^3 s^{-1} at 335 GeV after taking dSphs DM density profile uncertainties into account [50]. We expect improvements of this bound in the near future with more data taking. Note that we need non-thermal mechanism to achieve the observed relic DM density as the DM annihilation cross section is too large.

B. Model $XYB\phi$ with light B

In this subsection, we consider the $XYB\phi$ model in Table I, assuming $m_Y > m_X > m_B > m_\phi$. From the matter content in the table, the most generic renormalizable Lagrangian is

$$\mathcal{L} = \mathcal{L}_{SM} + \sum_{F=Y,X,B} \overline{F}(i\slashed{D} - m_F)F + \frac{1}{2}(\partial\phi)^2$$
$$- \frac{1}{2}m_\phi^2\phi^2 - V(H,\phi) - (\overline{Y}H)(\lambda_X + \lambda_{X5}\gamma_5)X$$
$$- \overline{B}(\lambda_B + \lambda_{B5}\gamma_5)(Y \cdot H) - y_{\phi i}\phi\overline{B}P_R d_{Ri} + \text{H.c.} \qquad (12)$$

where $(\overline{Y}H) = \overline{B}'H^+ + \overline{X}'H^0$ and $(Y \cdot H) = B'H^0 - X'H^+$. For simplicity, we assume $\lambda_{X5} = \lambda_{B5} = 0$. We further assume $y_{\phi 1} = y_{\phi 2} = 0$ and denote $y_{\phi 3} = y_\phi$.

The Yukawa couplings λ_X, λ_B and y_ϕ can be taken real and positive by field redefinitions. We also assume that the scalar interaction $V(H,\phi)$ does not affect DM abundance. The Yukawa couplings in (12) cause mixings between B and B', as well as between X and X', leading to mass eigenstates $B_{1,2}$ and $X_{1,2}$. Assuming $m_{X_2} \simeq m_{B_2} > m_{X_1} > m_{B_1} > m_\phi$ and $y_\phi \ll 1$, the main decay channels are given by

$$X_2 \to \begin{cases} B_1 W \\ X_1 Z, \\ X_1 h \end{cases} \qquad B_2 \to \begin{cases} X_1 W \\ B_1 Z, \\ B_1 h \end{cases}$$
$$X_1 \to B_1 W^*, \qquad B_1 \to b\phi. \qquad (13)$$

The mixings and decay rates of the fields are summarized in Appendix B 2.

1. Diphoton and ATLAS on-Z excesses

As discussed in Secs. II and III, this model may explain the diphoton and ATLAS on-Z excesses simultaneously.

(i) The decay rate of the X_1 is, using MADGRAPH [51], estimated as, for a benchmark point $(m_Y, m_X, m_B) \simeq (620, 375, 360)$ GeV,

$$\Gamma(X_1 \to B_1 + W^* \to B_1 + \ell\nu/jj)$$
$$\sim 10^{-6} \text{ GeV} \cdot \theta_X^2 \theta_B^2, \qquad (14)$$

with θ_X and θ_B being the mixing angles of the vectorlike quarks (see Appendix B). Therefore, it satisfies the condition for the diphoton excess, $\Gamma(X_1 \to b\eta^-) \ll \Gamma(S_0(X\overline{X}) \to \gamma\gamma) \simeq 1$ MeV, while avoiding the collider constraints for long-lived particles.

(ii) For the on-Z excess, let us first consider the case $\lambda_B \ll \lambda_X$. In this case, X_2 and B_2 mainly decays into $X_1 + Z/h$ and $X_1 + W$, respectively. The branching fraction Br$(X_2 \to X_1 Z)$ is essentially the same as the $XY\eta$ model discussed in Sec. IV A (see Fig. 4.) Thus, the on-Z excesses in run 1 and run 2 can be explained in a large region of parameter space. For $\lambda_B \sim \lambda_X$, the branching fraction Br$(X_2 \to X_1 + Z/h)$ decreases, but Br$(B_2 \to B_1 + Z/h)$ increases instead. The sum of them is close to unity up to kinematical corrections, and hence the result does not depend much on the hierarchy between λ_X and λ_B.

2. Other LHC constraints

We have also studied monojet bounds on the model $XYB\phi$ with light B. The monojet bounds are significantly stronger than the $XY\eta$ model since we now have a light B produced in pair recoiled against ISR as well. As a result, we do not find any parameter region that could avoid such

TABLE II.   Benchmarks for the $XYB\phi$ model with light B. The number of background (Bkg) and observed (Obs) events, as well as R_{obs} of the most sensitive signal region of each of the monojet analyses are shown [27,45,46]. The first benchmark corresponds to a parameter point where the thermal DM relic density matches the observed value ($\Omega_{DM}h^2 \simeq 0.12$). The second benchmark is a parameter point where, within our exploration, the monojet constraints are found to be least stringent.

(m_{DM}, m_B) [GeV]	SR	Bkg	Obs	R_{obs}
	2jm	163 ± 20	186	1.77
(320,365)	SR5	8300 ± 300	7988	0.79
	M2	8620 ± 270	8606	0.62
	2jm	163 ± 20	186	1.45
(305,365)	SR5	8300 ± 300	7988	0.66
	M2	8620 ± 270	8606	0.48

constraints. To show this, we fix $m_{X_1} = 375$ GeV, and choose two benchmarks: $(m_{DM}, m_B) = (320, 365)$, $(305, 365)$, where the numbers are in unit GeV. The first benchmark corresponds to a parameter point where the thermal relic DM density is achieved via coannihilation (see Sec. IV B 3). The second benchmark corresponds to a point where the monojet constraint is found to be the least stringent. Note that the $m_B - m_{DM}$ mass splitting of this benchmark is 60 GeV. The monojet constraints are further relaxed beyond 60 GeV but such a parameter region is excluded by the b-jets plus E_T^{miss} search (cf. Fig. 5). The results are shown in Table II. Again, it should be noted that there is a slight excess in the 13 TeV monojet signal region. Should the excess grow or persist in future LHC runs, this model would become relevant.

3. Dark Matter

DM-DM annihilation occurs via t-channel mediators and suffers from helicity suppression. The relic density of DM is instead determined by the annihilation rate of X_1 and B. This effect is characterized by the effective annihilation cross section [52]:

$$\sigma_{eff}v = \sum_{i=X_1,B} \sigma_i v \left(\frac{n_i^{eq}}{n^{eq}}\right)^2, \qquad (15)$$

where n_i^{eq} is the number density of particle i in thermal equilibrium, while n^{eq} is the sum of the number density of X_1, B and DM in thermal equilibrium. $\sigma_i v$ is the self-annihilation cross section of the fermion pairs, which is dominated by the QCD annihilation into a pair of gluons or quarks. We integrate the Boltzmann equation numerically to obtain the thermal relic DM density. In Fig. 7, we show the thermal relic DM density for some choices of mass splitting parameters. The parameter set $(m_{DM}, m_B, m_{X_1}) \simeq (320, 365, 375)$ GeV reproduces the observed relic DM density in the Universe.
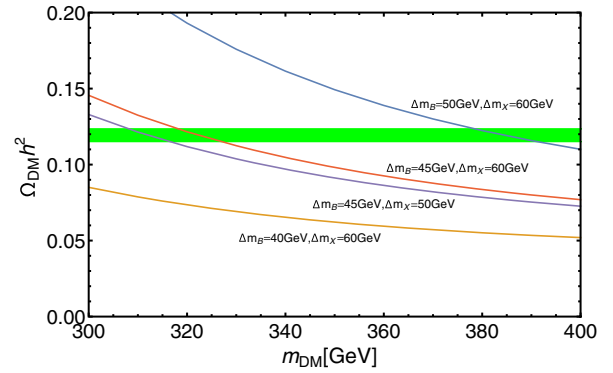

FIG. 7. $\Omega_{DM}h^2$ versus DM mass. Δm_X (Δm_B) is the mass difference between DM and X (B).

Let us briefly comment on the direct detection prospects of the model. As DM couples only to the bottom quark via B, the scattering of DM off a nucleon is only via loop-level interaction between DM and the nucleon's gluons. We found that the constraint on y_ϕ from the LUX experiment [53] is of $O(10)$ for B mass range of several hundred GeV to a few TeV. Probing the model with direct detection is extremely difficult.

C. Model $XYB\phi$ with quasidegenerate or heavy B

Finally, we consider the scenario where the Lagrangian is the same as (12), but with mass relations $m_B \gtrsim m_Y > m_X > m_\phi$. As we shall see, the minimal model would lead to a long lived X_1 at the collider scale, and we need additional new particles to make X_1 decay promptly.

The model where B is quasidegenerate with Y produces more on-Z signal events than the case where B is much heavier than Y or the inert scalar doublet scenario in Sec. IV A, as explained in Sec. III. Meanwhile, the X_1-DM mass splitting has to be small to avoid jets plus large E_T^{miss} constraints. As a result, two-body or three-body decay modes are kinematically closed within this minimal framework. X_1 can only decay via the following four-body decay mode: $X_1 \to W^* B_1^* \to jjj\phi$. However, the decay rate of this process is $\Gamma_{4-body} \lesssim 10^{-12}$ GeV $\cdot \theta_X^2 \theta_B^2$, which means that the colored and electrically charged X_1 typically decays outside the detector, leading to stringent collider constraints [10]. One is then forced to introduce new particle(s) to make X_1 decay promptly. One relatively simple possibility is to, instead of ϕ, consider fermion DM χ along with a color triplet scalar $\tilde{u}$ of quantum number $(\mathbf{3}, \mathbf{1}, 2/3)$. Assume the following interaction:

$$\Delta\mathcal{L} = \epsilon_{abc} y_X X^a \tilde{u}^b u^c + \delta_{ab} y_\chi \tilde{u}^{*a} u^b \chi + H.c., \quad (16)$$

where we have written down the color indices of the fields explicitly. The three-body decay rate is, based on dimensional analysis, $\Gamma_X \sim (y_X^2 y_\chi^2/128\pi^3)(m_X^5/m_{\tilde{u}}^4) \sim O(1)$ MeV

for $O(1)$ Yukawa couplings and $m_{\tilde{u}} = 1$ TeV. The formation of 750 GeV bound state requires $\Gamma_X \lesssim 1$ MeV, which translates to $m_{\tilde{u}} \gtrsim 1$ TeV for $O(1)$ Yukawa couplings.[7]

Let us briefly discuss other aspects of the χ model. Monojet constraints have been discussed in Ref. [8], where the X_1-DM mass splitting has to be $\gtrsim 30$ GeV. Let us assume that $\tilde{u}$ couples mainly to the top quark. The self-annihilation cross section of χ is, for $y_\chi \sim O(1)$ and $m_{\tilde{u}} \gtrsim 1$ TeV, $\sigma \simeq (y_\chi^4/32\pi)(m_t^2/m_{\tilde{u}}^4) \lesssim 3 \times 10^{-27}$ cm^3 s^{-1}, which is 1 order of magnitude smaller than the canonical thermal annihilation cross section. However, the self-annihilation of the slightly heavier X_1 can help reduce the relic density of χ. A mass splitting of around 40 GeV would lead to the correct value of the observed abundance of dark matter in the Universe. The prospect of direct detection is slim as χ couples to the third-generation quark. Indirect detection may be feasibe using the Cherenkov Telescope Array (CTA) [54]. Finally, the TeV-scale colored $\tilde{u}$ would be produced copiously at the LHC, and can be probed using standard techniques of SUSY searches.

V. SUMMARY AND DISCUSSION

Motivated by the LHC diphoton excess, we have considered some models involving a 750 GeV quarkonium, which is a bound state of vectorlike quarks X, in connection with dark matter and other excesses observed at the LHC. An exotic hypercharge of $Y_X = -4/3$ is required to fit the diphoton signal, indicating that there is additional particle(s) that mediates the decay of X in the full theory. We have introduced an SU(2) doublet vectorlike quark of mass around 600 GeV, and showed that not only the diphoton but also the on-Z excess (and potentially a slight excess in the monojet events) can be accommodated in our models.

Let us summarize the major findings of this paper. The three scenarios proposed here have distinctive properties, but all of them can accommodate the diphoton and on-Z excess. The scenario with inert scalar doublet (Sec. IV A) has inert scalar mass around 40 GeV below the 375 GeV diphoton-to-be vectorlike fermion X. As the annihilation cross section of DM is relatively large, non-thermal mechanism is needed to reproduce the correct DM relic density. On the flip side, the DM annihilation signals can optimistically be probed in near future. The second scenario (Sec. IV B) proposed in the paper involves the cascade decay of X into an almost degenerate bottomlike fermion, B, which in turn decays to DM. However, this model predicts too many monojet events. Even so, as there is currently a slight excess in the 13 TeV monojet channel,

this model should be given attention if the monojet excess persists or grows in the next run. The correct relic DM density is obtained via coannihilations with X and B. The third scenario (Sec. IV C) has B heavier than X. At certain mass region, the model can provide more on-Z signal events than the previous scenarios. However, in the minimal setup, X is unable to decay promptly. One needs to introduce a colored scalar triplet ($\tilde{u}$) to mediate the decay efficiently. This model may be tested with CTA by looking for the DM annihilation signals, or probed directly by searching for $\tilde{u}$ collider signatures at the LHC. The observed relic DM density is achieved via X coannihilation.

The observed diphoton excess has a relatively simple interpretation, i.e. a QCD bound state of heavy colored particles. We have argued that the full theory of such an interpretation can have rich collider and dark matter phenomenology. While the full theory necessitates the introduction of additional particles, we are encouraged by the fact these particles can provide ingredients to accommodate other LHC anomalies (on-Z, monojet). New experimental data, particularly from the next run of the LHC and dark matter indirect detection experiments (e.g. Fermi-LAT) will definitely test our proposal very soon.

APPENDIX A: EXPERIMENTAL ANALYSES

In this appendix, we describe the details of LHC analyses important to our study.

We begin with the ATLAS SUSY searches for final states containing an on-shell Z (on-Z) [11,12]. Both 8 and 13 TeV ATLAS on-Z analyses have the following requirements and cuts:
  (i) at least a pair of OSSF leptons with 81 GeV < m_{ll} < 101 GeV
  (ii) $E_T^{miss} > 225$ GeV
  (iii) number of jets $n_j \geq 2$
  (iv) $H_T > 600$ GeV
  (v) azimuthal distance between jets and $\not{p}_T$ $\Delta\phi(j, \not{p}_T) > 0.4$.

There are slight differences in the requirement of the p_T-ordered ith leptons ($p_T^{l_i}$) and jets ($p_T^{j_i}$). For the 8 TeV analysis:
  (i) $p_T^{l_1} > 25$ GeV, $p_T^{l_2} > 10$–14 GeV depending on trigger

---

[7]Note that, in this setup, the Y field does not play the role of mediating the X decay. The decay of X occurs through new scalar $\tilde{u}^{*a}$, while the ATLAS on-Z excess is explained by the decays of Y as well as B.

TABLE III.   Signal regions most sensitive to our studies. Notations are defined in text.

	E_T^{miss} [GeV]	p_{Tj_1} [GeV]	$\Delta\phi(j, \not{p}_T)$	n_j	H_T [GeV]	$E_T^{miss}/\sqrt{H_T}$	m_{eff} (incl.)	References
On-Z (8 TeV)	225	35	0.4	≥ 2	600	$\cdots$	$\cdots$	[11]
On-Z (13 TeV)	225	30	0.4	≥ 2	600	$\cdots$	$\cdots$	[12]
M2	340	340	0.4	≤ 3	$\cdots$	$\cdots$	$\cdots$	[45]
SR5	350	$0.5E_T^{miss}$	1.0	$\cdots$	$\cdots$	$\cdots$	$\cdots$	[46]
SR6	400	$0.5E_T^{miss}$	1.0	$\cdots$	$\cdots$	$\cdots$	$\cdots$	[46]
SR2jm	200	300	0.4	≥ 2	$\cdots$	15 GeV$^{1/2}$	1.2 TeV	[27]

(ii) $p_T^j > 35$ GeV

For the 13 TeV analysis:

   (i) $p_T^{l_1} > 50$ GeV, $p_T^{l_2} > 25$ GeV

   (ii) $p_T^j > 30$ GeV

Monojet searches have been performed by the ATLAS Collaboration to study SUSY with compressed mass spectra [45] and dark matter production at the LHC [46] at run 1. For [45], the following cuts are applied to all signal regions:

   (i) at least a jet with $p_T > 150$ GeV, i.e. $p_T^{j_1} > 150$ GeV

   (ii) $n_j \leq 3$ for jets with $p_T > 30$ GeV

   (iii) $E_T^{miss} > 150$ GeV

   (iv) $\Delta\phi(j, E_T^{miss}) > 0.4$ for all jets

   (v) no leptons with $p_T > 10$ GeV

Events passing these cuts are further divided into three signal regions M1–M3 which have additional requirements on E_T^{miss} and p_T^j. For the dark matter production monojet search [46]:

   (i) $p_T^{j_1} > 150$ GeV

   (ii) $p_T^{j_1}/E_T^{miss} > 0.5$

   (iii) $E_T^{miss} > 150$ GeV

   (iv) $\Delta\phi(j, E_T^{miss}) > 1.0$ for jets with $p_T > 30$ GeV

   (v) no leptons with $p_T > 7$ GeV

There are nine signal regions (SR1-9) corresponding to further different cuts on E_T^{miss} applying on events passing cuts above.

Furthermore, the run 2 SUSY search for squarks and gluino is placing strong monojet limits [27]. The relevant signal region is SR2jm and has kinematic cuts as follows:

   (i) $p_T^{j_1} > 300$ GeV

   (ii) $p_T^{j_2} > 50$ GeV

   (iii) $E_T^{miss} > 200$ GeV

   (iv) $\Delta\phi(j, E_T^{miss}) > 0.4$ up to three leading jets in the events

   (v) no leptons with $p_T > 10$ GeV

   (vi) $E_T^{miss}/\sqrt{H_T} > 15$ GeV$^{1/2}$

   (vii) $m_{eff} > 1600$ GeV,

where m_{eff} is defined as the sum of H_T and E_T^{miss}. We summarize signal regions sensitive to our models in Table III.

APPENDIX B: MIXINGS AND DECAY RATES OF VECTORLIKE QUARKS

In this appendix, we describe the mixings and decay rates of vectorlike quarks in the models discussed in Sec. IV.

1. Model $XY\eta$

Assuming $\lambda_{X5} = 0$, the mass terms of (X', X) in (7) become

$$-\mathcal{L}_{mass} = (\overline{X'}, \overline{X})\begin{pmatrix} m_Y & \lambda_X v \\ \lambda_X v & m_X \end{pmatrix}\begin{pmatrix} X' \\ X \end{pmatrix}, \quad (B1)$$

where $v = \langle H^0 \rangle \simeq 174$ GeV. It can be diagonalized by

$$\begin{pmatrix} X' \\ X \end{pmatrix} = \begin{pmatrix} \cos\theta_X & -\sin\theta_X \\ \sin\theta_X & \cos\theta_X \end{pmatrix}\begin{pmatrix} X_2 \\ X_1 \end{pmatrix}, \quad (B2)$$

where

$$\begin{aligned} \theta_X &= \frac{1}{2}\arctan\left(\frac{2\lambda_X v}{m_Y - m_X}\right) \\ &\simeq \frac{\lambda_X v}{m_Y - m_X} \\ &\simeq 0.07\left(\frac{\lambda_X}{0.1}\right)\left(\frac{250 \text{ GeV}}{m_Y - m_X}\right). \end{aligned} \quad (B3)$$

The mass splitting in the doublet, $m_{X_2} - m_{B'}$, is small for $\lambda_X \ll 1$:

$$m_{X_2} - m_{B'} \simeq \frac{(\lambda_X v)^2}{m_Y - m_X} \simeq 1.2 \text{ GeV}\left(\frac{\lambda_X}{0.1}\right)^2\left(\frac{250 \text{ GeV}}{m_Y - m_X}\right). \quad (B4)$$

The partial decay rates of X_2 are

$$\begin{aligned} \Gamma(X_2 \to X_1 Z) = \frac{1}{64\pi}\cos^2\theta_X \sin^2\theta_X \\ \times \frac{g_2^2 m_{X_2}^3}{m_W^2} f_V(r_1, r_Z)\overline{\beta}(r_1, r_Z) \end{aligned} \quad (B5)$$

$$\Gamma(X_2 \to X_1 h) = \frac{1}{32\pi}(\cos 2\theta_X)^2 \lambda_X^2 m_{X_2} f_h(r_1, r_h)\bar{\beta}(r_1, r_h)$$

(B6)

$$\Gamma(X_2 \to \eta^- b) = \frac{1}{32\pi}\cos^2\theta_X y_\eta^2 m_{X_2}(1 - r_\eta^2 + r_b^2)\bar{\beta}(r_\eta, r_b),$$

(B7)

where $r_1 = m_{X_1}/m_{X_2}$, $r_Z = m_Z/m_{X_2}$, $r_h = m_h/m_{X_2}$, $r_\eta = m_\eta/m_{X_2}$, and $r_b = m_b/m_{X_2}$. The functions f_V, f_h, and $\bar{\beta}$ are given by

$$f_V(r_1, r_V) = (1 - r_1^2)^2 + (1 - 6r_1 + r_1^2)r_V^2 - 2r_V^4,$$

(B8)

$$f_h(r_1, r_h) = 1 + 2r_1 + r_1^2 - r_h^2,$$

(B9)

$$\bar{\beta}(a, b) = \sqrt{1 + a^4 + b^4 - 2a^2 - 2b^2 - 2a^2 b^2}.$$

(B10)

In the limit of $m_Y - m_X \gg v$ and $\lambda_X \gg y_\eta$, the branching fractions become $\mathrm{Br}(X_2 \to X_1 Z) \simeq \mathrm{Br}(X_2 \to X_1 h) \simeq 0.5$, as expected from the Goldstone equivalence theorem.

The decay rate of the X_1 is given by

$$\Gamma(X_1 \to \eta^- b) = \frac{1}{32\pi}\sin^2\theta_X y_\eta^2 m_{X_1}(1 - r_{\eta 1}^2 + r_{b1}^2)\bar{\beta}(r_{\eta 1}, r_{b1}),$$

(B11)

where $r_{\eta 1} = m_\eta/m_{X_1}$ and $r_{b1} = m_b/m_{X_1}$. Finally, the decay rate of the η^- is given by [43]

$$\Gamma(\eta^- \to \eta^0 \pi^-) = \frac{G_F^2}{\pi}\cos^2\theta_c f_\pi^2 \Delta m^3 \sqrt{1 - m_{\pi^-}^2/\Delta m^2}.$$

(B12)

G_F is the Fermi constant. $\cos\theta_c$ is the Cabibo angle. f_π and m_{π^-} are the decay constant and mass of pion, respectively. Δm is the mass splitting between η^- and η^0.

2. Model $XYB\phi$

Assuming $\lambda_{X5} = \lambda_{B5} = 0$, the mass terms of (X', X) and (B', B) in (12) become

$$-\mathcal{L}_{\mathrm{mass}} = \sum_{F=X,B}(\bar{F}', \bar{F})\begin{pmatrix} m_Y & \lambda_F v \\ \lambda_F v & m_F \end{pmatrix}\begin{pmatrix} F' \\ F \end{pmatrix},$$

(B13)

where $v = \langle H^0 \rangle \simeq 174$ GeV. They can be diagonalized by

$$\begin{pmatrix} F' \\ F \end{pmatrix} = \begin{pmatrix} \cos\theta_F & -\sin\theta_F \\ \sin\theta_F & \cos\theta_F \end{pmatrix}\begin{pmatrix} F_2 \\ F_1 \end{pmatrix} \quad (F = X, B),$$

(B14)

where

$$\theta_F = \frac{1}{2}\arctan\left(\frac{2\lambda_F v}{m_Y - m_F}\right) \simeq \frac{\lambda_F v}{m_Y - m_F}$$

$$\simeq 0.07\left(\frac{\lambda_F}{0.1}\right)\left(\frac{250 \text{ GeV}}{m_Y - m_F}\right).$$

(B15)

The mass splitting in the doublet, $m_{X_2} - m_{B_2}$, is small for $\lambda_{B,F} \ll 1$:

$$m_{F_2} - m_Y \simeq \frac{(\lambda_F v)^2}{m_Y - m_F}$$

$$\simeq 1.2 \text{ GeV}\left(\frac{\lambda_F}{0.1}\right)^2\left(\frac{250 \text{ GeV}}{m_Y - m_F}\right)$$

$$(F = X, B).$$

(B16)

The partial decay rates of X_2 are

$$\Gamma(X_2 \to B_1 W) = \frac{1}{32\pi}\cos^2\theta_X \sin^2\theta_B$$

$$\times \frac{g_2^2 m_{X_2}^3}{m_W^2} f_V(r_{B_1}, r_W)\bar{\beta}(r_{B_1}, r_W)$$

(B17)

$$\Gamma(X_2 \to X_1 Z) = \frac{1}{64\pi}\cos^2\theta_X \sin^2\theta_X$$

$$\times \frac{g_2^2 m_{X_2}^3}{m_W^2} f_V(r_{X_1}, r_Z)\bar{\beta}(r_{X_1}, r_Z)$$

(B18)

$$\Gamma(X_2 \to X_1 h) = \frac{1}{32\pi}(\cos 2\theta_X)^2 \lambda_X^2 m_{X_2} f_h(r_{X_1}, r_h)$$

$$\times \bar{\beta}(r_{X_1}, r_h),$$

(B19)

where $r_{B_1} = m_{B_1}/m_{X_2}$, $r_W = m_W/m_{X_2}$, $r_{X_1} = m_{X_1}/m_{X_2}$, $r_Z = m_Z/m_{X_2}$, and $r_h = m_h/m_{X_2}$. The functions f_V, f_h, and $\bar{\beta}$ are given in Eqs. (B8)–(B10). The partial decay rates of B_2 are obtained by replacing X and B. In the limit of $m_Y - m_{X,B} \gg v$, the branching fractions become $\mathrm{Br}(X_2 \to B_1 W) \simeq C_B/(C_X + C_B)$ and $\mathrm{Br}(X_2 \to X_1 Z) \simeq \mathrm{Br}(X_2 \to X_1 h) \simeq (1/2) \cdot C_X/(C_X + C_B)$, where $C_F = \lambda_F^2(1 + r_F)^2(1 - r_F^2)$ $(F = B, X)$, as expected from the Goldstone equivalence theorem.

[1] G. Aad *et al.* (ATLAS Collaboration), Report No. ATLAS-CONF-2015-081.

[2] V. Khachatryan *et al.* (CMS Collaboration), Report No. CMS-PAS-EXO-15-004.

[3] G. Aad *et al.* (ATLAS Collaboration), Report No. ATLAS-CONF-2016-018.

[4] V. Khachatryan *et al.* (CMS Collaboration), Report No. CMS-PAS-EXO-16-018.

[5] M.-x. Luo, K. Wang, T. Xu, L. Zhang, and G. Zhu, Phys. Rev. D **93,** 055042 (2016).

[6] N. Craig, P. Draper, C. Kilic, and S. Thomas, Phys. Rev. D **93,** 115023 (2016).

[7] Y.-J. Zhang, B.-B. Zhou, and J.-J. Sun, arXiv:1602.05539.

[8] C. Han, K. Ichikawa, S. Matsumoto, M. M. Nojiri, and M. Takeuchi, J. High Energy Phys. 04 (2016) 159.

[9] Y. Kats and M. J. Strassler, J. High Energy Phys. 05 (2016) 092.

[10] M. Aaboud *et al.* (ATLAS Collaboration), Phys. Rev. D **93,** 112015 (2016).

[11] G. Aad *et al.* (ATLAS Collaboration), Eur. Phys. J. C **75,** 318 (2015), 75, 463(E) (2015).

[12] G. Aad *et al.*, Report No. ATLAS-CONF-2015-082.

[13] X. Lu, S. Shirai, and T. Terada, J. High Energy Phys. 05 (2016) 108.

[14] G. Barenboim, J. Bernabeu, V. A. Mitsou, E. Romero, and O. Vives, Eur. Phys. J. C **76,** 57 (2016).

[15] N. Vignaroli, Phys. Rev. D **91,** 115009 (2015).

[16] B. Allanach, A. Raklev, and A. Kvellestad, Phys. Rev. D **91,** 095016 (2015).

[17] U. Ellwanger, Eur. Phys. J. C **75,** 367 (2015).

[18] J. Cao, L. Shang, J. M. Yang, and Y. Zhang, J. High Energy Phys. 06 (2015) 152.

[19] A. Kobakhidze, N. Liu, L. Wu, and J. M. Yang, Phys. Rev. D **92,** 075008 (2015).

[20] M. Cahill-Rowley, J. L. Hewett, A. Ismail, and T. G. Rizzo, Phys. Rev. D **92,** 075029 (2015).

[21] X. Lu, S. Shirai, and T. Terada, J. High Energy Phys. 09 (2015) 204.

[22] S. P. Liew, A. Mariotti, K. Mawatari, K. Sakurai, and M. Vereecken, Phys. Lett. B **750,** 539 (2015).

[23] J. Cao, L. Shang, J. M. Yang, and Y. Zhang, J. High Energy Phys. 10 (2015) 178.

[24] R. Ding, Y. Fan, J. Li, T. Li, and B. Zhu, arXiv:1508.07452.

[25] K. Harigaya, M. Ibe, and T. Kitahara, J. High Energy Phys. 01 (2016) 030.

[26] M. Endo and Y. Takaesu, Phys. Lett. B **758,** 355 (2016).

[27] G. Aad *et al.* (ATLAS Collaboration), Report No. ATLAS-CONF-2015-062.

[28] Y. Kats and M. J. Strassler, J. High Energy Phys. 11 (2012) 097.

[29] M. Cacciari, G. P. Salam, and G. Soyez, J. High Energy Phys. 04 (2008) 063.

[30] J. Alwall, R. Frederix, S. Frixione, V. Hirschi, F. Maltoni, O. Mattelaer, H. S. Shao, T. Stelzer, P. Torrielli, and M. Zaro, J. High Energy Phys. 07 (2014) 079.

[31] J. Alwall, M. Herquet, F. Maltoni, O. Mattelaer, and T. Stelzer, J. High Energy Phys. 06 (2011) 128.

[32] T. Sjostrand, S. Mrenna, and P. Z. Skands, J. High Energy Phys. 05 (2006) 026.

[33] M. Drees, H. Dreiner, D. Schmeier, J. Tattersall, and J. S. Kim, Comput. Phys. Commun. **187,** 227 (2015).

[34] J. S. Kim, D. Schmeier, J. Tattersall, and K. Rolbiecki, Comput. Phys. Commun. **196,** 535 (2015).

[35] J. de Favereau, C. Delaere, P. Demin, A. Giammanco, V. Lemaître, A. Mertens, and M. Selvaggi (DELPHES 3 Collaboration), J. High Energy Phys. 02 (2014) 057.

[36] M. Cacciari, G. P. Salam, and G. Soyez, Eur. Phys. J. C **72,** 1896 (2012).

[37] M. Cacciari and G. P. Salam, Phys. Lett. B **641,** 57 (2006).

[38] A. Alloul, N. D. Christensen, C. Degrande, C. Duhr, and B. Fuks, Comput. Phys. Commun. **185,** 2250 (2014).

[39] M. Aliev, H. Lacker, U. Langenfeld, S. Moch, P. Uwer, and M. Wiedermann, Comput. Phys. Commun. **182,** 1034 (2011).

[40] G. Aad *et al.* (ATLAS Collaboration), J. High Energy Phys. 09 (2014) 176.

[41] K. Hamaguchi, S. P. Liew, T. Moroi, and Y. Yamamoto, J. High Energy Phys. 05 (2014) 086.

[42] M. Cirelli, N. Fornengo, and A. Strumia, Nucl. Phys. **B753,** 178 (2006).

[43] S. D. Thomas and J. D. Wells, Phys. Rev. Lett. **81,** 34 (1998).

[44] G. Aad *et al.* (ATLAS Collaboration), J. High Energy Phys. 10 (2013) 189.

[45] G. Aad *et al.* (ATLAS Collaboration), Phys. Rev. D **90,** 052008 (2014).

[46] G. Aad *et al.* (ATLAS Collaboration), Eur. Phys. J. C **75,** 299 (2015); **75,** 408(E) (2015).

[47] M. L. Mangano, M. Moretti, F. Piccinini, R. Pittau, and A. D. Polosa, J. High Energy Phys. 07 (2003) 001.

[48] M. L. Mangano, M. Moretti, F. Piccinini, and M. Treccani, J. High Energy Phys. 01 (2007) 013.

[49] J. Alwall *et al.*, Eur. Phys. J. C **53,** 473 (2008).

[50] M. Ackermann *et al.* (Fermi-LAT Collaboration), Phys. Rev. Lett. **115,** 231301 (2015).

[51] J. Alwall, C. Duhr, B. Fuks, O. Mattelaer, D. G. Özturk, and C.-H. Shen, Comput. Phys. Commun. **197,** 312 (2015).

[52] K. Griest and D. Seckel, Phys. Rev. D **43,** 3191 (1991).

[53] D. S. Akerib *et al.* (LUX Collaboration), Phys. Rev. Lett. **116,** 161301 (2016).

[54] M. Wood, J. Buckley, S. Digel, S. Funk, D. Nieto, and M. A. Sanchez-Conde, in *Community Summer Study 2013: Snowmass on the Mississippi (CSS2013) Minneapolis, 2013,* http://www.slac.stanford.edu/econf/C1307292.